◆ Human Brain Mapping 38:909–922 (2017) ◆

Subthalamic Nucleus Volumes Are Highly Consistent but Decrease Age-Dependently—A Combined Magnetic Resonance Imaging and Stereology Approach in Humans

Johann Zwirner,[1] Dustin Möbius,[1] Ingo Bechmann,[1] Thomas Arendt,[2] Karl-Titus Hoffmann,[3] Carsten Jäger,[2] Donald Lobsien,[3] Robert Möbius,[1] Uwe Planitzer,[4] Dirk Winkler,[4] Markus Morawski,[2] and Niels Hammer[1,5]*

[1]Faculty of Medicine, Institute of Anatomy University of Leipzig, Leipzig, Germany
[2]Paul-Flechsig-Institute for Brain Research University of Leipzig, Leipzig, Germany
[3]Department of Neuroradiology, University Clinic of Leipzig, Faculty of Medicine, Leipzig, Germany
[4]Department of Neurosurgery, University Clinic of Leipzig, Faculty of Medicine, Leipzig, Germany
[5]Department of Anatomy, University of Otago, Dunedin, New Zealand

Abstract: The subthalamic nucleus (STN) is a main target structure of deep brain stimulation (DBS) in idiopathic Parkinson's disease. Nevertheless, there is an ongoing discussion regarding human STN volumes and neuron count, which could potentially have an impact on STN-DBS. Moreover, a suspected functional subdivision forms the basis of the tripartite hypothesis, which has not yet been morphologically substantiated. In this study, it was aimed to investigate the human STN by means of combined magnetic resonance imaging (MRI) and stereology. STN volumes were obtained from 14 individuals (ranging from 65 to 96 years, 25 hemispheres) in 3 T MRI and in luxol-stained histology slices. Neuron number and cell densities were investigated stereologically over the entire STN and in pre-defined subregions in anti-human neuronal protein HuC/D-stained slices. STN volumes measured with MRI were smaller than in stereology but appeared to be highly consistent, measuring on average 99 ± 6 mm^3 (MRI) and 132 ± 20 mm^3 (stereology). The neuron count was 431,088 ± 72,172. Both STN volumes and cell count decreased age-dependently. Neuron density was different for the dorsal, medial and ventral subregion with significantly higher values ventrally than dorsally. Small variations in STN volumes in both MRI and stereology contradict previous findings of large variations in STN size. Age-dependent decreases in STN volumes and neuron numbers might influence the efficacy of STN-DBS in a geriatric population. Though the study is limited in sample size, site-dependent differences for the STN subregions form a morphological basis for the tripartite theory. *Hum Brain Mapp 38:909–922, 2017.*

Key words: 3 Tesla magnetic resonance imaging; deep brain stimulation; HuC/D; neuron density; stereology; tripartite hypothesis

*Correspondence to: Niels Hammer, M.D., Department of Anatomy, University of Otago, Lindo Ferguson Building, 270 Great King St, Dunedin 9016, New Zealand. E-mail: nlshammer@googlemail.com
Johann Zwirner and Dustin Möbius contributed as equally to this manuscript as first authors.
Markus Morawski and Niels Hammer contributed as equally to this manuscript as senior authors.

Received for publication 4 October 2015; Revised 8 September 2016; Accepted 26 September 2016.
DOI: 10.1002/hbm.23427
Published online 11 October 2016 in Wiley Online Library (wileyonlinelibrary.com)

INTRODUCTION

Deep brain stimulation (DBS) of the subthalamic nucleus (STN) is a routinely performed treatment in advanced idiopathic Parkinson's disease (IPD) [Benabid et al., 2000; Limousin and Martinez-Torres, 2008]. Although this method has been applied for a quarter of a century now [Benazzouz et al., 1993], side effects such as severe speech and voice disorders [Tsuboi et al., 2014], mania [Toker Ugurlu et al., 2014], suicides [Voon et al., 2008] and associated restrictions in patients' quality of life illustrate the need for further research in the field of DBS. Some side effects can be attributed to the reduction of dopaminergic drugs [Castrioto et al., 2014; Limousin et al., 1998], the suboptimal placement of electrodes [Benabid et al., 2009] or the spread of the electric current to adjacent structures [Castrioto et al., 2014] during stimulation. Reported STN volumes of the last 65 years give a first impression of the discrepancies in research varying from 20 mm^3 [Slavin et al., 2006] to 235 mm^3 [Schlaier et al., 2011]. If we take Marani's recalculation [Marani et al., 2008] of Richter's data [Richter et al., 2004] into account, a single STN can reach a maximum of 457 mm^3. Previously reported stereology-based volumes ranged from 120 mm^3 [Hardman et al., 2002] to 175 mm^3 [Hardman et al., 1997, 2002; Lévesque and Parent, 2005; Von Bonin and Shariff, 1951]. In magnetic resonance imaging (MRI) as state-of-the-art *in vivo* technique for visualizing the STN [Aviles-Olmos et al., 2014; Lefranc et al., 2014; Longhi et al., 2015; Schlaier et al., 2014], even larger discrepancies were reported, ranging from 42 mm^3 [Camlidag et al., 2014] to 235 mm^3 [Schlaier et al., 2014]. Based on the divergent volumes reported elsewhere, one could conclude that STN visualization might be less reliable in MRI than in histology or stereology [Weise et al., 2013].

Furthermore, the number of STN neurons in humans given in literature is based on few studies with very limited numbers of specimens, ranging from 239,500 [Lévesque and Parent, 2005] to 520,300 neurons [Füssenich, 1967]. In this context, the dependency of both volume and neuron count on age is an interesting aspect. As the STN is a grey matter structure, aging should be accompanied with a volumetric and cellular reduction due to neuronal loss [Giorgio et al., 2010; Sowell et al., 1999]. Shen and coworkers investigated a large sample size in MRI and found age-dependent decreases in STN volumes [Shen et al., 2009]. However, the age-dependent decreases in STN volumes could not be confirmed in other MRI-based studies [Keuken et al., 2013; Massey et al., 2012]. Also, concerning the number of STN neurons, no correlations were yet reported in relation to age [Lévesque and Parent, 2005]. Regarding brain atlases commonly used in DBS, age-dependent alterations in STN volumes would have implications concerning the target site.

Another aspect which could provide essential information for neurosurgeons is the functional and spatial subdivision of the STN into clearly distinguishable regions. The current leading hypothesis that the STN is divided into three subregions is widely spread and was recently demonstrated *in vivo* using diffusion weighted imaging [Lambert et al., 2012]. Since this assumption is based on few clinical observations or primate tracing studies, Alkemade and Forstmann stated that this hypothesis deserves re-evaluation [Alkemade and Forstmann, 2014].

Keuken et al. summarized 33 studies about the number of subthalamic subdivisions including non-human primates [Keuken et al., 2012]. They found scant evidence for the tripartite hypothesis whereas a division into two parts was adopted by two thirds [Keuken et al., 2012]. Moreover, they proposed ultra-high resolution MRI and histology to be the methods of choice to find evidence of assumed subdivisions within the human STN. While the selective stimulation of a certain sensomotoric subdivision within the STN remains attractive to alleviate motor symptoms in IPD, no histological evidence has to date been published supporting the tripartite hypothesis in humans. Morphologic differences in suspected subregions might be indicative of functionally different zones, which was our rationale to investigate the STN neuron density in predefined subvolumes. The goal of our investigation was therefore to provide an updated assessment of STN volumes in a direct MRI-histology comparison and related STN neuron densities.

The following hypotheses were addressed:

1. The STN is a volume-consistent structure both in MRI and related stereology.
2. STN volume and number of neurons are age-dependent.
3. Varying neuron densities provide morphological implications for the tripartite hypothesis of a subdivided STN.

MATERIAL AND METHODS

Dissection and STN Preparation

14 post-mortem human brains were obtained from body donors. While alive, all donors gave their informed and written consent to the donation of their bodies for teaching and research purposes. Being part of the body donor program regulated by the Saxonian Death and Funeral Act of 1994 (third section, paragraph 18 item 8), institutional approval for the use of the post-mortem tissues of human body donors was obtained from the Institute of Anatomy, University of Leipzig. The authors declare that all experiments have been conducted according to the principles of the Declaration of Helsinki. The mean age of the 4 male and 10 female body donors was 82.6 ± 10.0 years. The post-mortem delay was 24–72 hours (Table I). All brains were fixed in a mixture of 4-mass % paraformaldehyde (PFA) and 0.1 M phosphate-buffered saline (PBS; pH = 7.4) solution and stored away from light at 4°C. To prevent anatomical deformation the brains were suspended at the vessels of the circulus arteriosus cerebri. The PFA was

TABLE I. Clinical data on body donors used in this study

No.	Age (years)	Gender	Body weight (kg)	Brain weight (g)	Post-mortem delay (h)	Cause of death
1	65	F	98	1,123	24	Cancer of the biliary tree
2	69	F	64	1,304	72	Ovarian cancer
3	72	F	106	1,196	24	Sepsis
4	74	M	78	1,142	48	Sudden cardiac death
5	75	M	74	1,362	24	Acute kidney injury
6	81	F	56	1,186	24	Acute kidney injury
7	84	M	68	1,253	24	Subdural hematoma
8	85	F	64	1,126	24	Pulmonary edema
9	90	F	47	1,220	24	Cardiac insufficiency
10	90	F	84	1,344	24	Respiratory insufficiency
11	91	F	66	1,189	24	Heart attack
12	92	M	89	1,283	24	Heart attack
13	93	F	37	1,024	48	Cerebral infarction
14	96	F	67	1,336	24	Pneumonia
Mean value	82.6		71.3	1,220.6	30,85	
Standard deviation	10.0		18.8	98.7	14.67	

F, female; M, male.

changed once weekly to ensure optimal preservation of the specimens. After fixating the specimens for 30 days, tissue blocks including the STN and adjacent structures were removed from the brains. Therefore, a horizontal section was cut dorsal to the corpus callosum. Following this, a coronal section rostral to the optic chiasm was cut. Both hemispheres were then separated from the block sectioning lateral to the internal capsule. Caudally, a section in the axial plane just below the inferior colliculi defined boundaries.

MRI Acquisition

For MRI the PFA-fixed specimens were transferred to a plastic container. The bottom of the container was filled with gelatin (20-mass %) to minimize artifacts. The boxes were then filled with Fomblin (Y LVAC25/6; Solvay Solexis Inc., Bollate, Italy) according to Benveniste et al. [1999] and D'Arceuil et al. [2007]. The prepared containers including the specimens were evacuated to 14 mbar using a vacuum pump (VP0221; Busch Produktions GmbH, Maulburg, Germany) to remove air bubbles and dissolved air within the box and the specimens. The scanning procedure was performed at room temperature using a 3 T MRI scanner (Magnetom Trio, Siemens AG, Erlangen, Germany) and a 12 channel head coil. T2-weighted images were obtained [Connolly et al., 2012; Lefranc et al., 2014], using the following parameters: T2 turbo spin echo; isovoxel size 0.4 mm, imaging time = 144 min, TR = 1,000 ms, TE = 32 ms, number of averages = 3, number of connections = 1, flip angle = 87°, band width = 180 Hz/pixel, turbo factor = 15. The MRI data were analyzed using Mimics software (Materialise, Leuven, Belgium; Fig. 1). In both hemispheres the STN were outlined manually twice by two independent investigators (JZ, DM) blinded to each other's and their respective ratings before the volumes of each particular STN were calculated. These volumes were averaged and the obtained values were again averaged between the raters. Cronbach's alpha on the intra-rater reliability of the MRI-based STN volumes values was 0.89 ± 0.02. Cronbach's alpha on the inter-rater reliability of the MRI-based STN volumes was 0.77 ± 0.01. While segmenting in an axial plane, the internal capsule was used for defining the lateral border of the STN. In a coronal view the inferior and lateral aspect of the STN is bordered by the substantia nigra which was detected as a more hyperintense structure enveloping the ventral part of the STN. Sagitally, the superior-posterior border of the nucleus is demarcated by the zona incerta.

Histology

After MRI acquisition, the fixed specimens underwent a sequence of 70, 80, 96 and 100-volume % ethanol for dehydration. Subsequently the tissues were cleared in xylene for 16 hours with a renewal of the solvent after 8 hours. Dehydrating and clearing was performed on a shaking table with a gentle setting of 40 motions per minute. The blocks were preserved in paraffin with a melting point of 52°C–54°C for 12 hours followed by paraffin with a melting point of 56°C–58°C for 12 hours before they were embedded in paraffin. To evaluate shrinkage of the specimens, ten tissue blocks with a size similar to the samples were obtained from five of the PFA-fixed brains in proximity to the midbrain region. These blocks were treated in the same manner as the midbrain specimens. Volumes were determined before dehydrating the specimens in ethanol as well as after incubation in paraffin wax, measuring

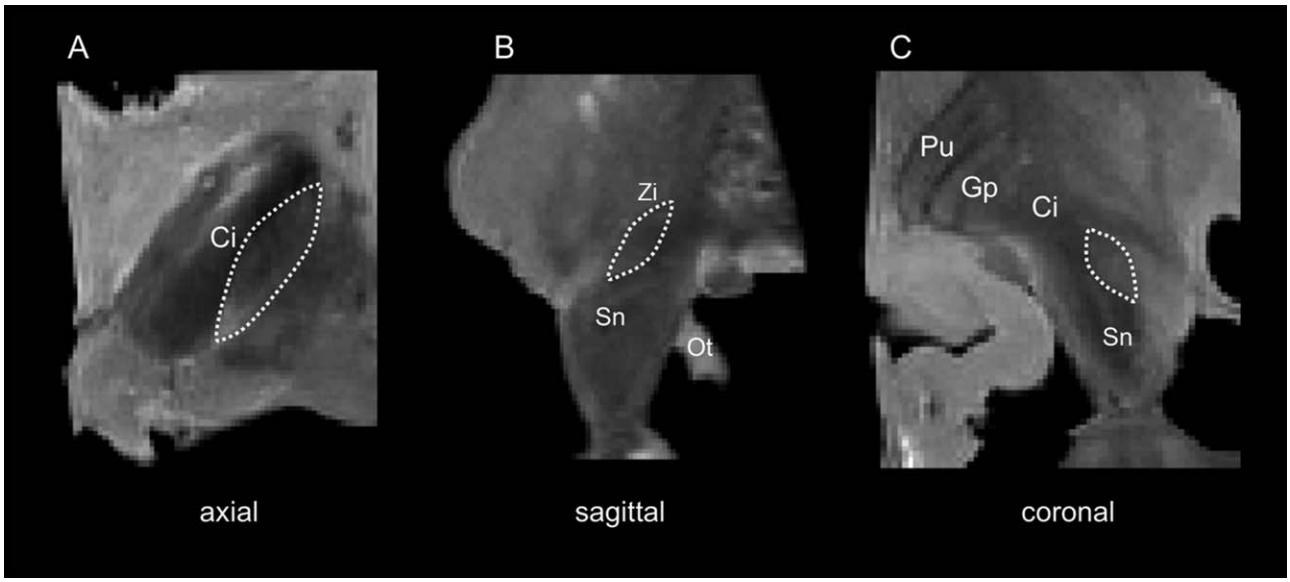

Figure 1.
T2-weighted magnetic resonance images of the human midbrain showing the subthalamic nucleus (STN). A: axial plane; B: sagittal plane; C: coronal plane; Ci, capsula interna; Gp, globus pallidus; Ot, optical tract; Pu, putamen; Sn, substantia nigra; Zi, zona incerta; dashed line, STN.

the displaced volume in 70-volume % ethanol and xylene, respectively. On basis of the shrinkage values, a correctional factor was computed to adjust the STN volumes in the histology specimens to the PFA-fixed condition.

Sections of 20 μm were obtained using a sliding microtome (Histoslide 2000R, Leica, Nussloch, Germany) similar to the study of Al-Helli and coworkers [Al-Helli et al., 2015]. The specimens were cut axially. The paraffin sections were dewaxed in xylene and rehydrated in a decreasing series of ethanol. One part of the sections was stained histochemically with luxol fast blue using cresyl fast violet as counter staining (luxol; Fig. 2A,B) [Klüver and Barrera, 1953]. Sections cut for immunohistochemical staining were pre-treated with an initial antigen retrieval step by heating to 90°C in trishydroxymethylamin-buffered saline (TRIS; pH = 8.0). Following a washing step with PBS-Tween (PBS-T) the sections were treated with 2-volume % hydrogen peroxide in 60-volume % methanol for 30 minutes to reduce endogenous peroxidase activity and rinsed with PBS-T. After that, a blocking step with 2% bovine serum albumin (Serva, Heidelberg, Germany), 0.5% donkey serum (Jackson Immuno Research, West Grove, PA) and 0.3% casein (Carl Roth GmbH, Karlsruhe, Germany) in PBS-T was performed for 30 minutes at room temperature to prevent non-specific antibody binding. Sections were incubated over two nights with primary antibody (1:500) at 4°C. Anti-human neuronal protein HuC/HuD mouse antibody 16A11 (HuC/D, Life Technologies, Darmstadt, Germany) was chosen to selectively stain the neurons [Marusich et al., 1994]. After incubation tissues were rinsed with PBS-T. Immunoreactivity was visualized using a secondary donkey-anti-rat IgG (H + L)-biotin antibody (Dianova, Hamburg, Germany). Following a washing step with PBS-T slices were incubated with an ExtrAvidin® peroxidase complex (Sigma, Munich, Germany). After PBS-T washing and rinsing with TBS the peroxidase binding was visualized by nickel-enhanced Diaminobenzidine (black) as a chromogen (Sigma, Munich, Germany) for 1–6 minutes. After one last washing step with PBS and TBS the sections were transferred into distilled water. Finally, sections were dehydrated in an increasing ethanol series, cleared in toluene, and mounted in Entellan (in toluene; Merck, Darmstadt, Germany).

Stereological Analysis

Stereological analysis was performed using the optical fractionator method according to West et al. [1991] and Morawski et al. [2012] to estimate numerical densities of HuC/D-stained neurons. The Stereo Investigator software (Version 7, MicroBright field, Williston, VT) was used and neuron counts were performed on a Zeiss Axioscop 2 plus (Zeiss, Jena, Germany) equipped with a motorized stage, a Ludl MAC 5000 (LEP, Hawthorne, NY) and a digital camera dv9000 (MicroBrightField, Williston, VT). The histological slices were segmented manually and neuron counts were performed by one rater. A final section thickness of 19.4 ± 2.4 μm was received on average. This permitted to a dissector height of 16 μm using a guard zone of 2 μm on either side of the section. HuC/D-stained sections were used every 200 ± 40 μm (corresponding to every 10th section) and luxol sections every 400 ± 40 μm (corresponding

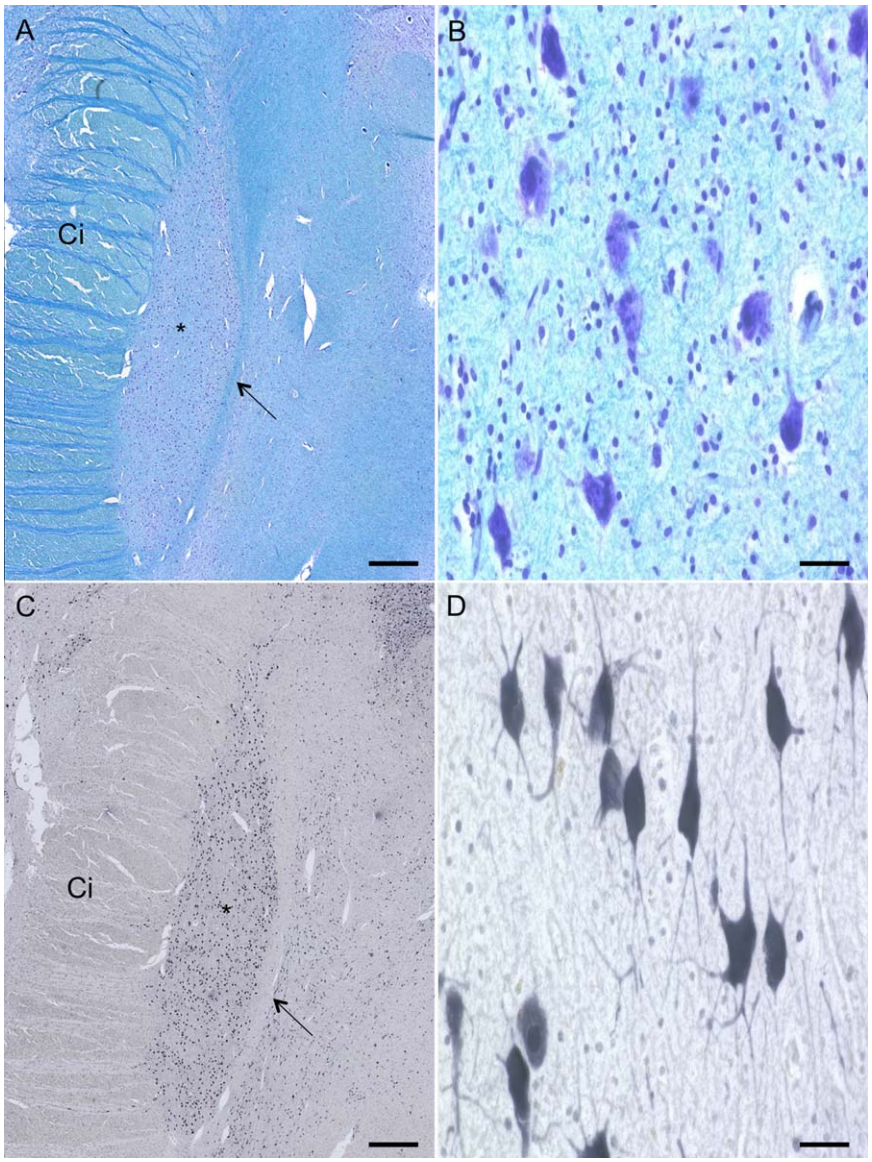

Figure 2.

Luxol-fast-blue-/cresyl-violet- and HuC/D-staining of the human subthalamic nucleus (STN). The STN (*) can be depicted as an almond shaped structure surrounded by the capsula interna (Ci) at its lateral border and zona incerta (arrow) at its medial border (A,C). Neurons in luxol staining appear less distinguishable and glia cells were stained (A,B). In the HuC/D-stained slices dendrites and axons of the neurons (C,D) are explicitly definable. Scale bar: 1,000 μm (A,C), 20 μm (B,D) [Color figure can be viewed at wileyonlinelibrary.com]

to every 20th section). Depending on the precise dimensions of each individual STN 25 ± 5 and 12 ± 3 sections per case were evaluated for the HuC/D and luxol staining, respectively. The STN was first outlined under 4× magnification and counting frames of 150 × 150 μm were placed systematically into the delineated area. To figure out a reliable grid size, a pilot study of six different grid sizes including the most accurate one of 150 × 150 μm was performed on one section. With an estimated deviation of less than one percent from the most precise value of 1,750 cells, a grid size of 400 × 400 μm was considered appropriate for further measurements. Neurons falling within these evenly distributed positions on the grid were then counted at 40× magnification (Fig. 2C,D). Cells were considered if they were explicitly stained and at least fifty percent of their soma and one dendritic branch was visible within the counting frame. Neurons, which did not fulfill these criteria, were excluded. The absolute number of

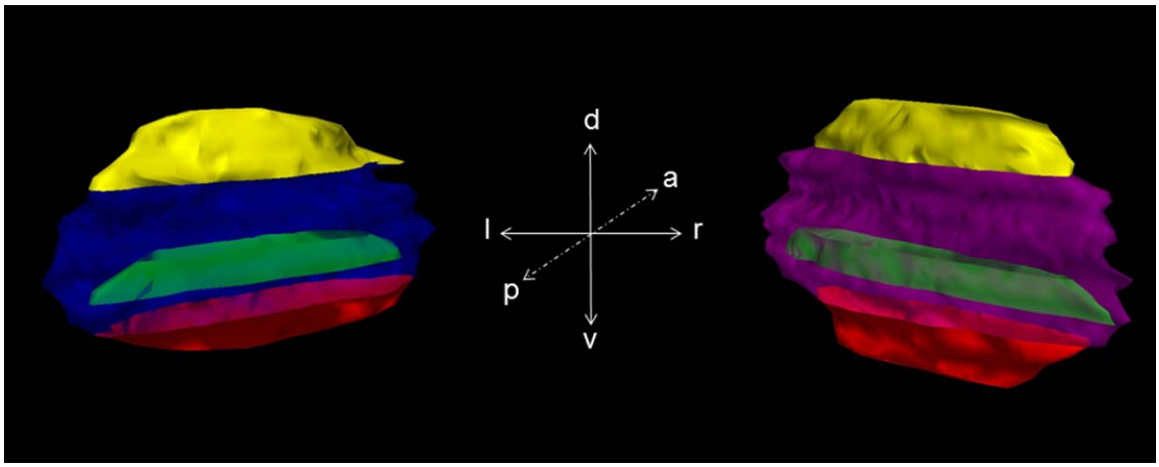

Figure 3.
The 3D reconstruction of the histological subthalamic nucleus (STN) from HuC/D-stained slices. Posterior view on the right and left STN including the predefined subvolumes. a: anterior; d: dorsal; l: left; p: posterior; r: right; v: ventral; yellow: dorsal subvolume; green: medial subvolume; red: ventral subvolume; blue: left STN; purple: right STN. [Color figure can be viewed at wileyonlinelibrary.com]

neurons N of each STN was evaluated with the following formula:

$$N = \sum Q^{-} \cdot \frac{t_2}{h} \cdot \frac{1}{asf} \cdot \frac{1}{ssf}$$

$\sum Q^{-}$ represents the total counts of neurons from each individual nucleus. Every 10th section was used, so the section sampling fraction (*ssf*) was 1/10. The area of the cumulated counting frame was 22,500 μm^2 and the associated area over the section surface was 160,000 μm^2, leading to an area sampling fraction (*asf*) of 0.14. The final section thickness after embedding and staining (t_2) resulted in 19.4 ± 2.4 μm. The height of the dissector (h) was 16 μm. The volume (V) of each STN was calculated with the following formula, using the Cavalieri method:

$$V = \sum A \cdot t_1 \cdot n.$$

$\sum A$ represents the total enclosed area of all sections sampled. The section thickness as determined by the microtome (t_1) was 20 μm. As every 10th section was sampled in HuC/D-stained slices and every 20th in luxol stained slices, n was 10, respectively, 20. The coefficient of error (CE) was calculated by the Stereo Investigator software as:

$$\mathrm{CE} = \frac{\sqrt{\left(\frac{1}{f} - \frac{1}{F}\right)s^2}}{\bar{Q}}$$

with the number of counting frames f, the total possible sampling sites F, the estimated variance s^2 and the average number of particles $\bar{Q}$. In our study the CE ranged from 0.015 to 0.070.

Delineation of the STN and Definition of Subvolumes

The STN is an almond shaped structure. With HuC/D staining a precise method was chosen to stain neurons selectively. In the luxol sections neurons were additionally counter-stained using cresyl fast violet. Both stainings allowed to differentiate the STN from adjacent structures. When cutting in an axial plane from dorsal to ventral the first neurons belonging to the STN were detected closely posterior to the lenticular fasciculus, which forms the superior border of the nucleus [Massey et al., 2012]. This fascicle can clearly be depicted both in HuC/D and in luxol-stained slices. The zona incerta (Fig. 2) runs alongside the posterior-medial border of the STN. The lateral border of the nucleus is formed by the internal capsule. Both zona incerta and internal capsule completely border the nucleus enabling to exactly define the superior and posterior aspect of the STN. The anterior and inferior part of the nucleus is formed by the substantia nigra (Sn) on the ventro-medial side and still by the internal capsule laterally. Subvolumes were placed in the dorsal, medial and ventral region of the STN (Fig. 3). These regions were much smaller than the presumed functional regions to ensure proper discrimination, averaging 5 mm^3 from consecutive slices as given from the Stereo Investigator software. The dorsal volume was defined by the very first consecutive slices containing STN neurons when cutting from dorsal to ventral. Respectively, when cutting in the described axis the last slices include the ventral part of the STN. For medial subvolumes we have chosen the slice showing the widest extension of the STN, which was close to the third ventricle. Segmentation was performed in this

slice as well as in one slice above and below. Therefore a line from the posterior to the anterior tip of the segmented STN area was drawn and areas even smaller than half of the STN were placed in this medial part of the nucleus.

Statistical Analyses

Microsoft Excel version 2010 (Microsoft Corporation, Redmond, WA) and SPSS version 20 (Chicago, IL) were used for statistical comparison. Cronbach's alpha was used to compare the intra- and inter-rater reliability of the volumes obtained from MRI. A Bland–Altman plot was utilized to compare the volumes derived from the MRI with stereology. Side- or gender-related differences were compared with the Kolmogorov–Smirnov test for equal distribution of the data, followed by an independent sample *t*-test with post correction using the Bonferroni method. A one-way ANOVA for multiple comparisons test with post-hoc analyses was used to compare cell densities within the subregions of the STN. Correlations were determined using Pearson's correlation coefficient (CC). *P* values of 0.05 or less were considered as statistically significant.

RESULTS

A total of 14 brain specimens (25 hemispheres) including the STN were processed by means of MRI and subsequent luxol staining. In six of these specimens, HuC/D-staining was performed with a focus on the STN. In three specimens, only one hemisphere could be investigated stereologically resulting from artifacts, which occurred while sectioning. Body weight and age did not vary significantly between the genders. Moderate age-dependent decreases in body weight were observed (CC = −0.48, $P = 0.01$). From the brain specimens taken to determine the shrinkage caused by the fixation and embedding, a volume decrease of 46% ± 5% was calculated, resulting in a correctional factor of 1.85.

Though STN Volumes Were Different in MRI and Stereology, STN Volumes Appear to Be Highly Consistent but Decreased with Age

The STN volumes in the MRI datasets averaged 99 ± 6 mm^3 (Fig. 4; Table II). In the luxol-stained slices, the STN volumes averaged 71 ± 11 mm^3 without shrinkage correction and 132 ± 20 mm^3 with shrinkage correction (Table II). Similar values were obtained in the HuC/D-stained samples with 68 ± 12 mm^3 and 126 ± 22 mm^3 without and with shrinkage correction, respectively. In each of the volumes obtained by the different methods, the variations in the STN volumes appeared to be small. Comparison of left and right STN volumes did not show differences on a statistically significant level. However, MRI-based STN volumes were significantly larger in females compared with males with 100.63 ± 5.82 mm^3 and 95.34 ± 8.86 mm^3, respectively ($P = 0.03$). The side difference was not statistically significant in the luxol-stained tissues (69.89 ± 9.28 vs. 72.97 ± 12.38 mm^3; $P = 0.08$). In the Bland–Altman plot comparing the volumes from MRI with the luxol-based volumes, differences of the mean values of 32.93 mm^3 were found (Fig. 5). Moreover, increasing STN volumes tended to give a larger spread between the single mean values obtained in both methods (CC = 0.851, $P < 0.01$). Moderate age-dependent decreases were observed for the stereology-based STN volumes in luxol (CC = −0.59, $P < 0.01$). Also, luxol-based STN volumes correlated negatively with brain weight (CC = −0.50, $P = 0.01$).

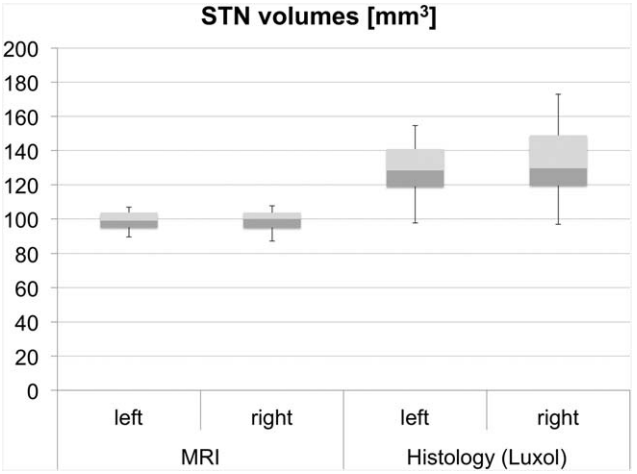

Figure 4.
Volumes of the subthalamic nucleus (STN) in magnetic resonance imaging (MRI) and histology. Volumes calculated from histology appear to be higher than those gained from MRI. The boxplots show the 25th percentile, median and the 75th percentile. The error bars reflect the minima and maxima.

The Number of STN Neurons Was Approximately 430,000 and Decreased Age-Dependently

The number of HuC/D-positive neurons in the STN region was on average 431,088 ± 72,172 cells. Side-comparison yielded non-significantly different results with 441,731 ± 82,821 and 418,317 ± 63,829 cells for the left and right side, respectively (Table III). Also, gender comparison revealed non-significantly neuron numbers for females and males with 390,426 ± 44,089 and 464,974 ± 76,362 cells, respectively. Moderate positive correlations were found for the cell count of HuC/D-positive STN neurons and STN volumes (CC = 0.68, $P = 0.02$). Moreover, a strong age-dependent decrease was observed in the cell count of HuC/D-positive STN neurons (CC = −0.75, $P < 0.01$).

Cell Density Varied Significantly in the Dorsal Compared with the Ventral STN Subvolumes

Within the predefined STN subvolumes, cell densities were as follows: in the dorsal region, density was 4,884 ± 1,321

TABLE II. Volumes of the subthalamic nucleus obtained from magnetic resonance imaging (MRI) and luxol fast blue/cresyl violet stained slices

	Subthalmic nucleus volume (mm^3)					
	MRI		Luxol		Luxol[a]	
No.	Left	Right	Left	Right	Left	Right
1	102.97	103.58	83.83	90.75	154.55	167.31
2	106.88	104.63	83.13	*	153.26	*
3	94.96	95.44	77.64	93.80	143.14	172.93
4	100.27	99.99	76.05	79.17	140.21	145.96
5	89.43	87.01	66.36	68.44	122.35	126.18
6	92.41	94.96	52.96	72.20	97.64	133.11
7	97.78	98.25	59.28	61.42	109.29	113.23
8	105.34	105.61	71.39	80.45	131.62	148.32
9	92.27	88.82	62.20	62.94	114.68	116.04
10	106.76	107.61	69.61	66.82	128.33	123.20
11	97.02	*	76.41	*	140.87	*
12	95.45	94.58	64.54	52.51	118.99	96.81
13	103.8	102.85	*	81.59	*	150.42
14	103.57	102.46	65.22	65.53	120.24	120.81
Mean ± SD	99.21 ± 5.80	98.91 ± 6.42	69.89 ± 9.28	72.97 ± 12.38	128.86 ± 17.10	134.52 ± 22.82
Total	99.06 ± 5.99		71.37 ± 10.76		131.58 ± 19.83	

[a], corrected with shrinkage factor; SD, standard deviation; *, excluded due to artifacts.

cells/mm^3, in the medial region, cell density was 6,345 ± 913 cells/mm^3. In the ventral region, density averaged 8,000 ± 2,169 cells/mm^3 (Fig. 6; Table III) Cell densities did not vary side- or gender-dependently on a statistically significant level. Comparison between the three subregions showed significantly lower cell densities in the dorsal compared with the ventral region ($P < 0.001$) as tested with the ANOVA followed by post-hoc testing. Comparison of the cell density of the ventral region compared with the medial region ($P = 0.06$) and comparison of the dorsal to the medial region ($P = 0.11$) yielded non-significant differences. No age- or body weight-dependent alterations were observed in the cell densities.

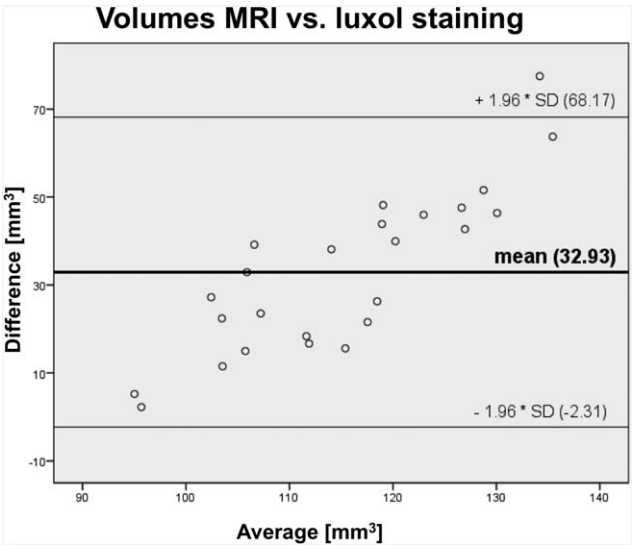

Figure 5.
Bland–Altman plot comparing the volumes obtained from magnetic resonance imaging with histology. The plot indicates that methods give different but consistent results with increasing errors at increasing volumes.

DISCUSSION

A glance at literature reveals that 150 years after Jules Bernard Luys first characterized the STN [Luys, 1865], several fundamentals of this small diencephalic structure, such as a functional subdivision, are still open to debate [Keuken et al., 2012; Lambert et al., 2012]. Our study is the first to substantiate STN volumes in a correlative 3 T T2-weighted MRI and stereology approach. Both methods were proven to give different but consistent results, indicated by the Bland-Altman plots (Fig. 5). In our study, STN volumes were obtained stereologically in a sample size of 25 STN, which is higher than in previous studies with one to fourteen STN [Füssenich, 1967; Hardman et al., 1997, 2002; Lange et al., 1976; Lévesque and Parent, 2005; Von Bonin and Shariff, 1951].

STN Volumes Are Highly Consistent in Stereology and Decrease Age-Dependently

The STN volumes determined with the luxol staining were highly consistent among the samples from the different individuals of our group. Our obtained STN volumes confirm the

TABLE III. Numbers of neurons obtained from stereological analysis and calculated neuron densities within the predefined subvolumes

			Neuron density (cells/mm^3)					
	Neuron count		Dorsal		Medial		Ventral	
No.	Left	Right	Left	Right	Left	Right	Left	Right
4	572,054	483,361	4,189	3,328	5,609	5,660	8,239	6,677
7	484,303	487,669	5,061	7,412	7,272	6,668	9,389	10,252
9	321,438	379,175	2,784	6,442	7,837	4,853	5,558	5,023
10	416,136	346,323	4,396	5,293	6,243	7,592	9,395	10,533
11	425,994	*	4,198	*	6,025	*	4,538	*
14	430,465	395,062	5,173	5,451	5,904	6,132	8,885	9,507
Mean ± SD	441,731 ± 82,821	418,318 ± 63,829	4300 ± 857	5,585 ± 1,522	6,482 ± 874	6,181 ± 1,033	7,667 ± 2,098	8,398 ± 2,428
Total	431,089 ± 72,172		4884 ± 1321		6,345 ± 913		8,000 ± 2,169	

SD, standard deviation; *, excluded due to artifacts.

results of the Hardman group (single STN ~ 124 mm^3) which applied comparable pre-conditions for the stereological analysis [Hardman et al., 1997, 2002]. Further, our data support the older work of the Lange group reporting volumes of approximately 139 mm^3 [Lange et al., 1976]. However, Von Bonin and Shariff [1951] as well as Lévesque and Parent [2005] reported larger volumes from 157 to 175 mm^3, respectively. Possible explanations for the deviation in STN volumes from our data might be related to the different methods applied and also to the sample sizes being much smaller in their study. During the embedding process, we observed volume decreases of approximately 46% compared with the initial volume, which was our rationale to adjust the STN volumes for shrinkage. Vice versa, STN volumes are unlikely to be smaller than the minimum volumes computed from the embedded samples without adjusting these data for shrinkage (Fig. 4; Table II). Taking into account the unadjusted minimum values and age-dependent decreases of the geriatric population under investigation shown here, it is highly unlikely for STN volumes *in vivo* to have values less than our lowest reported STN volume of 53 mm^3. Although, even smaller values have been reported elsewhere but appear to be the effects of estimations [Akakin et al., 2015; Camlidag et al., 2014; Schäfer et al., 2012; Slavin et al., 2006]. Conclusively, STN volume can be considered consistent in both MRI and stereology, confirming our first hypothesis.

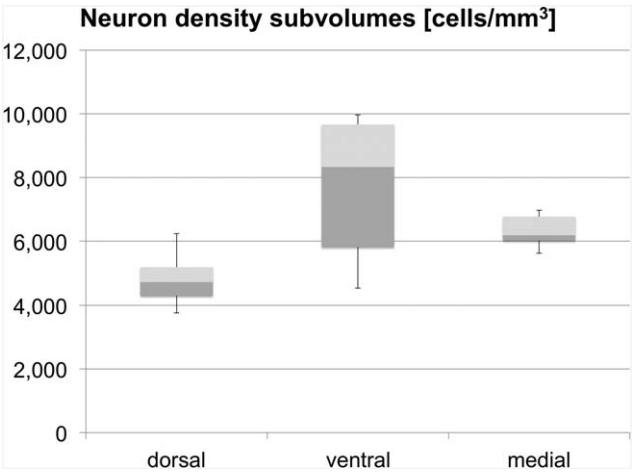

Figure 6.
Neuron densities in predefined subvolumes within the human subthalamic nucleus (STN). Densities calculated in the dorsal subregion of the STN were significantly lower than those in the ventral part. The boxplots show the 25th percentile, median and the 75th percentile. The error bars reflect the minima and maxima.

Another relevant finding in our study was that STN volume significantly decreased with age, confirming our second hypothesis. Though this finding is in accordance with an expected age-dependent atrophy of grey matter structures [Giorgio et al., 2010; Sowell et al., 1999], it has not yet been proven for the STN stereologically. Earlier histological studies on age-dependent alterations of STN volume could not substantiate this finding [Hardman et al., 1997, 2002; Lévesque and Parent, 2005]. Our finding of brain-weight dependent decreases in STN volumes cannot be entirely explained on the basis of the given data and needs further substantiation in a functional context.

MRI Volumes Complement the Volumes Obtained from Histology

In accordance to published literature, MRI-based human STN volumes show large variations, ranging between 42 mm^3 [Camlidag et al., 2014] and 235 mm^3 [Schlaier et al., 2011]. Table IV summarizes existing investigations on STN volumes. In contrast to the existing values reported in these studies, the MRI-based STN volumes in our study were considerably consistent (Table II). Additionally, in spite of the fact that the manual STN volume rendering appears to introduce a measurement error largely dependent on the investigator's experience, intra- and

TABLE IV. Comparison of subthalamic nucleus (STN) volumes published in literature

Author	Method	Age (mean age)	Age range (years)	Volume (mm^3)	Segmentation
Our values	*MRI 3.0 T*	*83*	*65–96*	*99*[a]	*SA*
Our values	*Histology (20 μm paraffin)*	*83*	*65–96*	*131*	*SA*
Akakin et al., 2015 [retracted]	n/g	n/g	n/g	40	n/g
Xiao et al., 2014	MRI 3.0 T	61	n/g	156[b]	SA
Camlidag et al., 2014	MRI 1.5 T	56	45–65	42[a,c]	SA
Keuken et al., 2014	MRI 7.0 T	24	n/g	56[d]	SA
Weiss et al., 2015	MRI 7.0 T	67	44–91	109[d]	SA
Keuken et al., 2013	MRI 7.0 T	24	22–28	62[d]	SA
Keuken et al., 2013	MRI 7.0 T	51	40–59	75[d]	SA
Keuken et al., 2013	MRI 7.0 T	72	67–77	52[d]	SA
Lambert et al., 2012	MRI 3.0 T	34	n/g	155[e]	SA
Massey et al., 2012	MRI 9.4 T	75	38–94	106	SA
Schäfer et al., 2012	MRI 7.0 T	24	22–28	48	SA
Forstmann et al., 2012	MRI 7.0 T	24	18–33	58[d]	SA
Schlaier et al., 2011	MRI 1.5 T	63	46–73	235	SA
Colpan and Slavin, 2010	MRI 3.0 T	62	n/g	270	SA
Shen et al., 2009	MRI 1.5 T	♂:44; ♀: 46	21–80	132[f]	SA
Nowinski et al., 2006	NURBS-reconstruction	n/g	atlas-based	174[g]	A
Slavin et al., 2006	n/g	n/g	n/g	20	SA
Lévesque and Parent, 2005	Histology (55 μm freezing microtome)	51	22–85	175	SA
Richter et al., 2004	MRI 1.5 T	55	39–68	60[h]	M
Richter et al., 2004	MRI 1.5 T	55	39–68	457[i]	M
Hardman et al., 2002	Histology (50 μm cryostat)	74	n/g	120[j]	SA
Yelnik, 2002	Computer-aided 3D cartography	n/g	n/g	158	A
Hardman et al., 1997	Histology (50 μm cryostat)	75	61–84	127[j]	SA
Schaltenbrand and Wahren, 1977	Atlas of stereotaxy	n/g	atlas-based	183[k]	M
Lange et al., 1976	Histology (20 μm paraffin)	50	24–99	139[l]	M
Füssenich, 1967	Histology (20 μm paraffin)	70	58–91	64	M
von Bonin and Shariff, 1951	Histology	n/g	n/g	157	M

[a]Volume calculation is based on average mask of raters.
[b]AC-PC native space.
[c]Proportion of the entire brain volume.
[d]Volume calculation is based on conjuction mask of raters.
[e]Average of left and right STN volumes.
[f]Average of male and female STN volumes including both hemispheres.
[g]Average of volumes obtained from axial, coronal, and sagittal models.
[h]Recalculation of Schäfer et al. [2012].
[i]Recalculation of Marani et al. [2008].
[j]Given total STN volume of both hemispheres divided by 2.
[k]Approximated by Nowinski et al. [2005].
[l]Average of male and female STN volumes; A—"automatic": segmentation is fully based on a computer software without manual segmentation as a part of the process; M—"manual": no computer software was involved in the segmentation process and in volume calculating; MRI—magnetic resonance imaging; n/g—not given; NURBS—Nonuniform Rational B-Splines; SA—"semiautomatic": segmentation is done manually and a computer software (e.g., Neurolucida, Image J) was used to calculate the volume.

inter-individual ratings proved our results to be reliable. Determining the STN volumes from MRI is influenced by several factors, like quality of images (acquisition time, field strength, image weighting and size) which might crucially influence outlining the STN shape [Kerl et al., 2012; Massey et al., 2012; Weise et al., 2013]. However, even if imaging conditions were similar the obtained volumes varied widely [Camlidag et al., 2014; Schlaier et al., 2011], which is in contrast to our data. Consequently, MRI-based segmentations are highly affected by the conventions of the research groups regarding what is recognized to be the STN in MRI. This issue is related to so-called "problem zones" which are difficult to visualize even with excellent imaging parameters, no matter if using a 1.5 T or a 9.4 T MRI scanner [Massey et al., 2012; Rijkers et al., 2007].

Contrary to stereology, MRI volumes of the STN revealed no correlation with age. Shen and colleagues have shown

age-dependent decreases of STN volumes [120 participants, range 20–80 years, 1.5 T MRI scanner; Shen et al., 2009]. They observed volume decreases from approximately 135 mm^3 (20–30 years) to approximately 122 mm^3 (70–80 years) in their cohorts. The body donors used in our study had a mean age of 83 ± 10 years. This age is significantly older than the mean age at first diagnosis of IPD averaging 60 years [Samii et al., 2004]. Patients with an average age as in our study usually present symptoms if suffering from IPD. Therefore, we consider our sample likely to be valid as a non-IPD control. Taking this into account, the MRI-based volumes of 99 ± 6 mm^3 obtained in our study complement the age-dependent decreases of the STN volumes reported by Shen et al. [2009]. Massey et al. obtained volumes of 106 mm^3 per STN in 9.4 T MRI [Massey et al., 2012]. Female STN volumes obtained in MRI were significantly larger than male ones, contradicting the findings of Shen et al. [2009]. The fact that we could not substantiate age-related changes of STN volumes in MRI may be related to the limited resolution in our setting. Also the above-mentioned difficulties in outlining the STN and the relatively low case number within an age span ranging between 65 and 96 years might be a reason. Abosch et al. showed a highly improved demarcation of the STN to surrounding structures *in vivo* obtained in a 7 T scanner using susceptibility-weighted imaging [Abosch et al., 2010]. Moreover, Cho et al. could significantly prove the advantages of 7 T MR images regarding spatial resolution and contrast to adjacent tissues compared with 1.5 and 3 T MRI [Cho et al., 2010]. These points enhance the need for ultra-high field MRI to visualize the STN both in anatomical as well as in clinical settings.

The Number of STN Neurons Appears to Be Higher than Reported Recently and Decreases with Age

An average number of 431,000 neurons was computed for a single STN in our study based on stereological investigations in HuC/D-stained slices. HuC/D is selectively staining neuron-specific RNA. The number of false-negative neurons or false-positive cells is low compared with Nissl or other histochemical stains. Consequently, the number of neurons computed from histology appears to be quite accurate [Marusich et al., 1994]. Most recent investigations using Nissl staining report lower STN neuron numbers. Lévesque et al. computed 239,500 neurons per STN in 5 male hemispheres [Lévesque and Parent, 2005]. Hardman and coworkers reported similar values of approximately 280,000 neurons in 5 brains [Hardman et al., 1997, 2002]. The largest number of STN samples was investigated by Lange et al., determining 297,000 STN neurons within 14 hemispheres [Lange et al., 1976]. The highest numbers of STN neurons were reported by Füssenich with 530,000 cells in 5 brains [Füssenich, 1967]. To our best knowledge our study is the first to report significant decreases of STN neuron count with age. This number is in line with a continuous loss of neurons accompanied with normal ageing [Terry et al., 1987] and might have an impact on the STN as a target site in deep brain stimulation for the treatment of IPD.

Neuron Density in Subvolumes Appears to Be Site Dependent, Forming a Morphological Basis for the Tripartite Theory of the STN

Lambert et al. [2012] as well as Haynes and Haber [2013] gave evidence for the existence of a topologically-organized STN in humans and in primates, respectively. Furthermore, they argue that there is no strict anatomical border between the suspected parts of the STN. In our study, while examining the histological slices, we could not detect any evidence for a physical border between the neurons such as septa. Addressing the tripartite hypothesis, neuron density was determined in three predefined regions within the STN (Figs. 3 and 6). These were a dorsal, medial and ventral subregion. In our experiments, investigating neuron densities within the respective regions, significant differences were observed between the dorsal and the ventral part of the STN. These data expand the findings of Lévesque et al. describing an increase in cell density from the dorsal to the ventral part of the STN [Lévesque and Parent, 2005]. Such an idea of a gradient as well as the differences of neuron density we observed within the predefined subvolumes might be an anatomical implication for a subdivision of the STN. These findings need to be substantiated *in vivo*.

Moreover, both the shape and volumetric analyses of STN neurons were not in focus of our investigation. In future studies it is therefore necessary to analyze the STN neurons in the subvolumes with regard to their potential function as well as their morphological characteristics. Even though imaging methods like diffusion weighted imaging, fiber tracking or MRI using higher field strengths provide proper evidence for a subdivided STN, we still consider histology to be the basis of investigation. Combining both methods will therefore expand the results in future research. One of our hypotheses stating that the functional separation of the STN is reflected by differences in STN morphology can therefore be accepted in part - comparing the dorsal with the ventral subregion.

Though Age-Dependent Decline in STN Volumes and Neuron Number Was Observed, the STN Appears to Be a Highly Consistent Structure for DBS Due to the Small Variation in Volume

Our study reveals decline of human STN volume and cell count with age (ranging between 65 and 96 years). Independent of STN changes, which may be affected functionally and structurally by Parkinson's disease itself [Bronstein et al., 2011; Samii et al., 2004], the natural decrease of STN volume and neuron count with age could be an influencing factor on the efficacy and the side effects

following DBS. The demonstrated age-dependency could result in a lower number of neurons in the target region. This fact and the findings on the STN shifting in an age-dependent manner [Den Dunnen and Staal, 2005; Kitajima et al., 2008; Mavridis et al., 2014] might also influence the efficacy of STN-DBS especially if the STN is localized indirectly [Savas et al., 2013; Schuepbach et al., 2013]. Moreover, the smaller the STN, the more precise the accuracy of electrode placing should be in order to have the desired clinical effects. Electrode placement in a smaller structure might as well be influenced by intraoperative brain-shift [Winkler et al., 2005], which is likely to increase age-dependently due to cortical atrophy. However, based on our theoretical investigations, the neurosurgeon may expect a consistent STN volume of 132 ± 20 mm^3 in the subthalamic region. The accuracy in which the STN was visualized in our experiments may however not be realized in a clinical setting due to the extremely long image acquisition times. Therefore, in quite a few cases the STN is not clearly definable in clinical routine due to e.g. low scanning time, resulting in indirect [Schuepbach et al., 2013] rather than in direct targeting [Houshmand et al., 2014; Lefranc et al., 2014; Longhi et al., 2015; Savas et al., 2013]. Nevertheless, knowing that the STN is a consistent structure concerning its volume may explain the reliability of DBS in most cases.

Limitations

First, the brains used in this study were obtained from elderly and therefore mostly multimorbid donors. Severity of diseases, premortal pharmacological treatments as well as post-mortem delay might influence the tissue quality. To minimize these effects, we carefully screened our donors and excluded the ones with known neurological disorders. In all 14 specimens no neurodegenerative changes could be observed histologically. Moreover, we only used brains with a relatively short post mortem delay (maximum 72 hours), undergoing subsequent cooling post mortem. Secondly, even though we calculated an adjustment factor to compensate for the shrinkage following the embedding of the tissues, it remains unclear whether the shrinkage occurring within the STN is different from the surrounding tissues. Inhomogeneous shrinkage could partly explain the differences between the stereology- and the MRI-based volumes. It also needs to be taken into account that the post-mortem magnetic properties of tissues change with prolonged fixation [Shepherd et al., 2009]. Thirdly, despite using a guarding zone for the cell count, it cannot be excluded that the stereological results might be affected in terms of an over-estimation of neurons, which has to be weighed against a slight underestimation in HuC/D staining. Finally, the predefined subvolumes used to investigate neuron densities only partly reflect the layout of subdivisions commonly proposed in literature [Hamani et al., 2004; Joel and Weiner, 1997; Massey and Yousry, 2010; Parent and Hazrati, 1995; Smith et al., 1990; Temel et al., 2006]. Especially the medial subregion in our observations extends far more into the center of the nucleus than described there.

ACKNOWLEDGMENTS

The authors would like to express their gratitude to the body donors for donating their corpses for this research project after passing away. The authors also thank their families for supporting their valuable decision. Dr. Reinhard Braul from MIcroBrightfield kindly supported us with the 3D reconstruction and analysis of the stereological data. Furthermore, we would like to acknowledge Sabine Löffler, Uwe Deubel and Matthias Oehme for their support obtaining the tissues.

REFERENCES

Abosch A, Yacoub E, Ugurbil K, Harel N (2010): An assessment of current brain targets for deep brain stimulation surgery with susceptibility-weighted imaging at 7 tesla. Neurosurgery 67:1745–1756.

Akakin A, Yilmaz B, Kilic T, Rhoton AL Jr (2015): Anatomy of the subthalamic nucleus, with correlation of deep brain stimulation. J Neurosurg [recently retracted by the author due to anatomical incorrectness; doi:10.3171/2014.10.JNS145].

Alkemade A, Forstmann BU (2014): Do we need to revise the tripartite subdivision hypothesis of the human subthalamic nucleus (STN)?. Neuroimage 95:326–329.

Al-Helli O, Thomas DL, Massey L, Foltynie T, Limousin P, Holton JL, Yousry TA, Zrinzo L (2015): Deep brain stimulation of the subthalamic nucleus: Histological verification and 9.4-T MRI correlation. Acta Neurochir 157:2143–2147.

Aviles-Olmos I, Kefalopoulou Z, Tripoliti E, Candelario J, Akram H, Martinez-Torres I, Jahanshahi M, Foltynie T, Hariz M, Zrinzo L, Limousin P (2014): Long-term outcome of subthalamic nucleus deep brain stimulation for Parkinson's disease using an MRI-guided and MRI-verified approach. J Neurol Neurosurg Psychiatry 85:1419–1425.

Benabid AL, Koudsie A, Benazzouz A, Fraix V, Ashraf A, Le Bas JF, Chabardes S, Pollak P (2000): Subthalamic stimulation for Parkinson's disease. Arch Med Res 31:282–289.

Benabid AL, Chabardes S, Mitrofanis J, Pollak P (2009): Deep brain stimulation of the subthalamic nucleus for the treatment of Parkinson's disease. Lancet Neurol 8:67–81.

Benazzouz A, Gross C, Féger J, Bourad T, Bioulac B (1993): Reversal of Rigidity and Improvement in Motor Performance by Subthalamic High-frequency Stimulation in MPTP-treated Monkeys. Eur J Neurosci 5:382–389.

Benveniste H, Einstein G, Kim KR, Hulette C, Johnson GA (1999): Detection of neuritic plaques in Alzheimer's disease by magnetic resonance microscopy. Proc Natl Acad Sci U S A 96:14079–14084.

Bronstein JM, Tagliati M, Alterman RL, Lozano AM, Volkmann J, Stefani A, Horak FB, Okun MS, Foote KD, Krack P, Pahwa R, Henderson JM, Hariz MI, Bakay RA, Rezai A, Marks WJ, Jr, Moro E, Vitek JL, Weaver FM, Gross RE, DeLong MR (2011): Deep brain stimulation for Parkinson disease: An expert consensus and review of key issues. Arch Neurol 68:165.

Camlidag I, Kocabicak E, Sahin B, Jahanshahi A, Incesu L, Aygun D, Yildiz O, Temel Y, Belet U (2014): Volumetric analysis of

the subthalamic and red nuclei based on magnetic resonance imaging in patients with Parkinson's disease. Int J Neurosci 124:291–295.

Castrioto A, Lhommee E, Moro E, Krack P (2014): Mood and behavioural effects of subthalamic stimulation in Parkinson's disease. Lancet Neurol 13:287–305.

Cho ZH, Min HK, Oh SH, Han JY, Park CW, Chi JG, Kim YB, Paek SH, Lozano AM, Lee KH (2010): Direct visualization of deep brain stimulation targets in Parkinson disease with the use of 7-tesla magnetic resonance imaging. J Neurosurg 113: 639–647.

Colpan ME, Slavin KV (2010): Subthalamic and red nucleus volumes in patients with Parkinsons disease: Do they change with disease progression? Parkinsonism and Realted. Disorders 16:398–403.

Connolly PJ, Halpern CH, Baltuch GH, Danish SF, Jaggi JL (2012): Implications for programming strategy of the location of the active contact in subthalamic nucleus deep brain stimulation. J Clin Neurosci 19:1029–1031.

D'Arceuil HE, Westmoreland S, de Crespigny AJ (2007): An approach to high resolution diffusion tensor imaging in fixed primate brain. Neuroimage 35:553–565.

Den Dunnen WFA, Staal MJ (2005): Anatomical Alterations of the Subthalamic Nucleus in Relation to Age: A Postmortem Study. Mov Disord 20(7).

Forstmann BU, Keuken MC, Jahfari S, Bazin PL, Neumann N, Schafer A (2012): Cortico-subthalamic white matter tract strength predict interindividual efficacy in stopping a motor response. NeuroImage 60:370–375.

Füssenich M (1967): Vergleichend anatomische Studien über den Nucleus subthalamicus (Corpus Luys) bei Primaten. In: Frieburg, C.O.V.I.f.H.A.-L.-U., editor. Dissertation.

Giorgio A, Santelli L, Tomassini V, Bosnell R, Smith S, De Stefano N, Johansen-Berg H (2010): Age-related changes in grey and white matter structure throughout adulthood. Neuroimage 51:943–951.

Hamani C, Saint-Cyr JA, Fraser J, Kaplitt M, Lozano AM (2004): The subthalamic nucleus in the context of movement disorders. Brain 127:4–20.

Hardman CD, Halliday GM, McRitchie DA, Morris JG (1997): The subthalamic nucleus in Parkinson's disease and progressive supranuclear palsy. J Neuropathol Exp Neurol 56:132–142.

Hardman CD, Henderson JM, Finkelstein DI, Horne MK, Paxinos G, Halliday GM (2002): Comparison of the basal ganglia in rats, marmosets, macaques, baboons, and humans: Volume and neuronal number for the output, internal relay, and striatal modulating nuclei. J Comp Neurol 445:238–255.

Haynes WI, Haber SN (2013): The organization of prefrontal-subthalamic inputs in primates provides an anatomical substrate for both functional specificity and integration: Implications for Basal Ganglia models and deep brain stimulation. J Neurosci 33:4804–4814.

Houshmand L, Cummings KS, Chou KL, Patil PG (2014): Evaluating indirect subthalamic nucleus targeting with validated 3-tesla magnetic resonance imaging. Stereotact Funct Neurosurg 92:337–345.

Joel D, Weiner I (1997): The connections of the primate subthalamic nucleus: Indirect pathways and the open-interconnected scheme of basal ganglia-thalamocortical circuitry. Brain Res Brain Res Rev 23:62–78.

Kerl HU, Gerigk L, Pechlivanis I, Al-Zghloul M, Groden C, Nolte IS (2012): The subthalamic nucleus at 7.0 Tesla: Evaluation of sequence and orientation for deep-brain stimulation. Acta Neurochir 154:2051–2062.

Keuken MC, Uylings HB, Geyer S, Schäfer A, Turner R, Forstmann BU (2012): Are there three subdivisions in the primate subthalamic nucleus?. Front Neuroanat 6:14.

Keuken MC, Bazin PL, Schäfer A, Neumann J, Turner R, Forstmann BU (2013): Ultra-high 7T MRI of structural age-related changes of the subthalamic nucleus. J Neurosci 33:4896–4900.

Keuken MC, Bazin PL, Crown L, Hootsmans J, Laufer A, Müller-Axt C, Sier R, van der Putten EJ, Schäfer A, Turner R, Forstmann BU (2014): Qunatifying inter-individual anatomical variability in the subcortex using 7T structural MRI. NeuroImage 94:40–46.

Kitajima M, Korogi Y, Kakeda S, Moriya J, Ohnari N, Sato T, Hayashida Y, Hirai T, Okuda T, Yamashita Y (2008): Human subthalamic nucleus: evaluation with high-resolution MR imaging at 3.0 T. Neuroradiology 50:675–681.

Klüver H, Barrera E (1953): A method for the combined staining of cells and fibers in the nervous system. J Neuropathol Exp Neurol 12:400–403.

Lambert C, Zrinzo L, Nagy Z, Lutti A, Hariz M, Foltynie T, Draganski B, Ashburner J, Frackowiak R (2012): Confirmation of functional zones within the human subthalamic nucleus: Patterns of connectivity and sub-parcellation using diffusion weighted imaging. NeuroImage 60:83–94.

Lange H, Thorner G, Hopf A (1976): Morphometric-statistical structure analysis of human striatum, pallidum and nucleus su-thalamicus. III. Nucleus subthalamicus. J Hirnforsch 17:31–41.

Lefranc M, Derrey S, Merle P, Tir M, Constans JM, Montpellier D, Macron JM, Le Gars D, Peltier J, Baledentt O, Krystkowiak P (2014): High-resolution 3-dimensional T2*-weighted angiography (HR 3-D SWAN): an optimized 3-T magnetic resonance imaging sequence for targeting the subthalamic nucleus. Neurosurgery 74:615–626.

Lévesque JC, Parent A (2005): GABAergic interneurons in human subthalamic nucleus. Movement Disord 20:574–584.

Limousin P, Martinez-Torres I (2008): Deep brain stimulation for Parkinson's disease. Neurotherapeutics 5:309–319.

Limousin P, Krack P, Pollak P, Benazzouz A, Ardouin C, Hoffmann D, Benabid AL (1998): Electrical stimulation of the subthalamic nucleus in advanced Parkinson's disease. N Engl J Med 339:1105–1111.

Longhi M, Ricciardi G, Tommasi G, Nicolato A, Foroni R, Bertolasi L, Beltramello A, Moretto G, Tinazzi M, Gerosa M (2015): The role of 3t magnetic resonance imaging for targeting the human subthalamic nucleus in deep brain stimulation for parkinson disease. J Neurol Surg a Cent Eur Neurosurg 76:181–189.

Luys, JB (1865): Recherches sur le système nerveux cérébro-spinal, sa structure, ses fonctions et ses maladies. Paris. J.B. Baillière et fils.

Marani E, Heida T, Lakke EAJF, Usunoff KG (2008): The subthalamic nucleus. Part I: Development, cytology, topography and connections. Adv Anat Embryol Cell Biol 198:1–113.

Marusich MF, Furneaux HM, Henion PD, Weston JA (1994): Hu neuronal proteins are expressed in proliferating neurogenic cells. J Neurobiol 25:143–155.

Massey LA, Yousry TA (2010): Anatomy of the substantia nigra and subthalamic nucleus on mr imaging. Neuroimag Clin N Am 20:7–27.

Massey LA, Miranda MA, Zrinzo L, Al-Helli O, Parkes HG, Thornton JS, So PW, White MJ, Mancini L, Strand C, Holton JL, Hariz MI, Lees AJ, Revesz T, Yousry TA (2012): High resolution MR anatomy of the subthalamic nucleus: Imaging at 9.4 T with histological validation. Neuroimage 59:2035–2044.

Mavridis I, Boviatsis E, Anagnostopoulou S (2014): Stereotactic anatomy of the human subthalamic nucleus: Providing coordinates for accurate electrode placement. J Neurol Surg a Cent Eur Neurosurg 75:289–298.

Morawski M, Bruckner G, Jager C, Seeger G, Matthews RT, Arendt T (2012): Involvement of perineuronal and perisynaptic extracellular matrix in Alzheimer's disease neuropathology. Brain Pathol 22:547–561.

Nowinski WL, Belov D, Pollak P, Benabid AL (2005): Statistical analysis of 168 bilateral subthalamic nucleus implantations by means of the probabilistic functional atlas. Neurosurgery 57 (ONS suppl 3):319–330.

Nowinski WL, Liu J, Thirunavuukarasuu A (2006): Quantification and visualization of the three-dimensional inconsistency of the subthalamic nucleus in the Schaltenbrand-Wahren brain atlas. Stereotact Funct Neurosurg 84:46–55.

Parent A, Hazrati LN (1995): Functional anatomy of the basal ganglia. II. The place of subthalamic nucleus and external pallidum in basal ganglia circuitry. Brain Res Rev 20:128–154.

Richter EO, Hoque T, Halliday W, Lozano AM, Saint-Cyr JA (2004): Determining the position and size of the subthalamic nucleus based on magnetic resonance imaging results in patients with advanced Parkinson disease. J Neurosurg 100:541–546.

Rijkers K, Temel Y, Visser-Vandewalle V, Vanormelingen L, Vandersteen M, Adriaensens P, Gelan J, Beuls EA (2007): The microanatomical environment of the subthalamic nucleus. Technical note. J Neurosurg 107:198–201.

Samii A, Nutt JG, Ransom BR (2004): Parkinson's disease. Lancet 363:1783–1793.

Savas A, Bozkurt M, Akbostanci C (2013): A comparison between stereotactic targeting methods of the subthalamic nucleus in cases with Parkinson's disease. Acta Neurochir Suppl 117:35–41.

Schäfer A, Forstmann BU, Neumann J, Wharton S, Mietke A, Bowtell R, Turner R (2012): Direct visualization of the subthalamic nucleus and its iron distribution using high-resolution susceptibility mapping. Hum Brain Mapp 33:2831–2842.

Schaltenbrand, G, Wahren, W (1977): Atlas for Stereotaxy of the Human Brain. Stuttgart: Thieme.

Schlaier JR, Habermeyer C, Warnat J, Lange M, Janzen A, Hochreiter A, Proescholdt M, Brawanski A, Fellner C (2011): Discrepancies between the MRI- and the electrophysiologically defined subthalamic nucleus. Acta Neurochir 153:2307–2318.

Schlaier JR, Hanson C, Janzen A, Fellner C, Hochreiter A, Proescholdt M, Brawanski A, Lange M (2014): Deep brain stimulation in Parkinson's disease: Motor effects relative to the MRI-defined STN. Neurosurg Rev 37:461–470.

Schuepbach WM, Rau J, Knudsen K, Volkmann J, Krack P, Timmermann L, Halbig TD, Hesekamp H, Navarro SM, Meier N, Falk D, Mehdorn M, Paschen S, Maarouf M, Barbe MT, Fink GR, Kupsch A, Gruber D, Schneider GH, Seigneuret E, Kistner A, Chaynes P, Ory-Magne F, Brefel Courbon C, Vesper J, Schnitzler A, Wojtecki L, Houeto JL, Bataille B, Maltete D, Damier P, Raoul S, Sixel-Doering F, Hellwig D, Gharabaghi A, Kruger R, Pinsker MO, Amtage F, Regis JM, Witjas T, Thobois S, Mertens P, Kloss M, Hartmann A, Oertel WH, Post B, Speelman H, Agid Y, Schade-Brittinger C, Deuschl G, Group ES (2013): Neurostimulation for Parkinson's disease with early motor complications. N Engl J Med 368:610–622.

Shen WG, Wang HY, Lin ZG, Shen H, Chen XG, Fu YL, Gao WP (2009): Stereotactic localization and visualization of the subthalamic nucleus. Chin Med J (Engl) 122:2438–2443.

Shepherd TM, Thelwall PE, Stanisz GJ, Blackband SJ (2009): Aldehyde fixative solutions alter the water relaxation and diffusion properties of nervous tissue. Magn Reson Med 62:26–34.

Slavin KV, Thulborn KR, Wess C, Nersesyan H (2006): Direct visualization of the human subthalamic nucleus with 3T MR imaging. AJNR Am J Neuroradiol 27:80–84.

Smith Y, Hazrati LN, Parent A (1990): Efferent projections of the subthalamic nucleus in the squirrel monkey as studied by the PHA-L anterograde tracing method. J Comp Neurol 294: 306–323.

Sowell ER, Thompson PM, Holmes CJ, Batth R, Jernigan TL, Toga AW (1999): Localizing age-related changes in brain structure between childhood and adolescence using statistical parametric mapping. Neuroimage 9:587–597.

Temel Y, Kessels A, Tan S, et al. (2006): Behavioural changes after bilateral subthalamic stimulation in advanced Parkinson disease: A systematic review. Parkinsonism Relat Disord 12:265–272.

Terry RD, DeTeresa R, Hansen LA (1987): Neocortical cell counts in normal human adult aging. Ann Neurol 21:530–539.

Toker Ugurlu T, Acar G, Karadag F, Acar F (2014): Manic Episode Following Deep Brain Stimulation of the Subthalamic Nucleus for Parkinson's Disease: A Case Report. Turk Neurosurg 24:94–97.

Tsuboi T, Watanabe H, Tanaka Y, Ohdake R, Yoneyama N, Hara K, Nakamura R, Watanabe H, Senda J, Atsuta N, Ito M, Hirayama M, Yamamoto M, Fujimoto Y, Kajita Y, Wakabayashi T, Sobue G (2014): Distinct phenotypes of speech and voice disorders in Parkinson's disease after subthalamic nucleus deep brain stimulation. J Neurol Neurosurg Psychiatry 1–9.

Von Bonin G, Shariff GA (1951): Extrapyramidal nuclei among mammals; a quantitative study. J Comp Neurol 94:427–438.

Voon V, Krack P, Lang AE, Lozano AM, Dujardin K, Schüpbach M, D'Ambrosia J, Thobois S, Tamma F, Herzog J, Speelmann JD, Samanta J, Kubu C, Rossignol H, Poon Y, Saint-Cyr JA, Ardouin C, Moro E (2008): A multicentre study on suicide outcomes following subthalamic stimulation for Parkinson's disease. Brain 131:2720–2728.

Weise LM, Seifried C, Eibach S, Gasser T, Roeper J, Seifert V, Hilker R (2013): Correlation of active contact positions with the electrophysiological and anatomical subdivisions of the subthalamic nucleus in deep brain stimulation. Stereotact Funct Neurosurg 91:298–305.

Weiss M, Alkemade A, Keuken MC, Muller-Axt C, Geyer S, Turner R, Forstmann BU (2015): Spatial normalization of ultrahigh resolution 7 T magnetic resonance imaging data of the postmortem human subthalamic nucleus: A multistage approach. Brain Struct Funct 220:1695–1703.

West MJ, Slomianka L, Gundersen HJ (1991): Unbiased stereological estimation of the total number of neurons in thesubdivisions of the rat hippocampus using the optical fractionator. Anat Rec 231:482–497.

Winkler D, Tittgemeyer M, Schwarz J, Preul C, Strecker K, Meixensberger J (2005): The first evaluation of brain shift during functional neurosurgery by deformation field analysis. J Neurol Neurosurg Psychiatry 76:1161–1163.

Xiao Y, Jannin P, D'Albis T, Guizard N, Haegelen C, Lalys F, Vérin M, Collins DL (2014): Investigation of morphometric variability of subthalamic nucleus, red nucleus, and substantia nigra in advanced parkinson's disease patients using automatic segmentation and pca-based analysis. Hum Brain Mapp 35: 4330–4344.

Yelnik J (2002): Functional anatomy of the basal ganglia. Mov Disord 17 Suppl 3:S15–S21.